Detection and localization of gold nanoshells inside cells: Near-Field approximation

MARIO D'ACUNTO[1,2,*], ANTONIO CRICENTI[2], SERENA DANTI[3], SIMONE DINARELLI[2], MARCO LUCE[2], DAVIDE MORONI[1], OVIDIO SALVETTI[1]

[1] *Consiglio Nazionale delle Ricerche, Istituto di Scienza e Tecnologie dell'Informazione, CNR-ISTI, via Moruzzi 1, 56124, Pisa. Italy.*
[2] *Consiglio Nazionale delle Ricerche, Istituto di Struttura della Materia, CNR-ISM, via Fosso del Cavaliere, 100, 00133 Rome, Italy*.
[3] *Dept. of Surgical, Medical, Molecular Pathology and Emergency Medicine, University of Pisa, via Paradisa 2, 56124, Pisa, Italy*
*Corresponding author: mario.dacunto@ism.cnr.it

Abstract: The optical properties of metal nanoparticles play a fundamental role for their use in a wide range of applications. In hyperthermia treatment, for example, the gold nanoshells (NSs, dielectric core + gold shell) pre-embedded in a cancer cell absorb energy when exposed to appropriate wavelengths of a laser beam and heat up thus destroying the cancer cell. In this process, nevertheless, the healthy tissues (not targeted by the NSs) along the laser path are not affected; this is because most biological soft tissues have a relatively low light absorption coefficient in the near-infrared (NIR) regions, characteristic known as the tissue optical window. Over such window, NIR light transmits through the tissues with the scattering-limited attenuation and minimal heating avoiding damages to the healthy tissues. As a consequence, the identification of NSs assumed a fundamental role for the further development of such cancer treatment. Recently, we have demonstrated the possibility to identify 100-150nm diameter gold NSs inside mouse cells using a scanning near-optical microscope (SNOM). In this paper, we provide numerical demonstration that the SNOM is able to locate NSs inside the cell with a particle-aperture distance of about 100nm. This result was obtained developing an analytical approach based on the calculation of the dyadic Green function in near-field approximation. The implications of our findings will remarkably affect further investigations on the interaction between NSs and biological systems.

***OCIS codes:** (180.4243) Near-field Microscopy; (260.3060) Infrared; (240.6680) Surface Plasmons; (300.1030) Absorption.*

1. INTRODUCTION

The optical properties of metallic (e.g., gold, silver) nanoparticles in the visible and near-infrared (Vis-NIR) domains are based on the collective response of conduction electrons, the so-called plasmon excitations [1-4]. These form an electron gas that moves away from its equilibrium position when perturbed by an external light field, inducing surface polarization charges that act as a restoring force on the electron gas. The result is a collective oscillatory motion of the electrons characterized by a dominant resonance band that, depending by the shape and size of the metal nanoparticles, falls in the Vis-NIR range [1]. Plasmons produce strong effects in both the near- and far-field response of metal nanoparticles, essentially, gold and silver. The far-field is fundamental for describing the macroscopic properties of absorption and scattering in colloidal dispersions and metamaterials. The near-field properties, instead, play a key role in describing the surroundings of the particle within a distance smaller than the wavelength of light, i.e., the optical properties between nanoparticles, the interaction with nearby molecules and the sensing powering as in the SERS techniques [5]. Just as an example, the near-field properties of gold NSs can act as nanolens with near-field enhancements that vary from 3 times for gold nanoshells with outer radii of 12-15nm, up to an enhancement factor of ~450 for assemblies of gold nanospheres that can be thought as made of

rows of nanolenses [1]. Since two decades, the near-field is experimentally detected via scanning near-field optical microscopy (SNOM) [6].

One biomedical application where a combination of NSs, NIR transparency window and near-field optics plays a fundamental role, face the problem of identification of NSs inside cells. The ability to identify NSs inside cells is of vital importance for medical treatments of cancers, as well as for the investigation of inner cell organs and components [7-9]. Recently, we demonstrated the possibility to identify 100-150nm diameter gold NSs inside mouse cells using an aperture SNOM [10].

In this paper, we numerically demonstrated that a SNOM with an aperture diameter of nearly 50nm is able to locate NSs inside the cell with a particle-aperture distance of about 100nm. This result is obtained developing an analytical approach based on the calculation of the dyadic Green function in near-field approximation, and it is in good agreement on what expected by a SNOM with a $\lambda/10$ resolution.

2. THE NEAR-FIELD OPTICAL PROPERTIES OF GOLD NS AS OBSERVED BY AN APERTURE SNOM

The optical cross-sections and luminescent properties of gold nanoshells compare favorably with those of conventional

fluorophores or quantum dots [11-14]. The NIR power absorption of a single 20-nm diameter nanoshell can correspond to the equivalent absorption of 4×10^4 molecules of a common dye, like the indocyanine green, used as a photosensitizer in photodynamic therapy [15]. But the most important characteristic of gold nanoshells is their tunability, in fact the position of the extinction peak correspondent to the plasmon resonance and the selective contributions of absorption and scattering to total extinction can be tuned changing only two parameters: the radii of the inner core and the outer shell. This tunability is particularly important if we wish to exploit the NIR tissue window from 700 to 900nm, where tissues are most transparent to light. The tunability in the NIR of barium titanate-gold NS (80nm core+ 40nm gold shell) was recently demonstrated using Mie scattering [16-17] and the possibility to identify such NSs inside mouse cells was later evidenced experimentally using an aperture SNOM [10]. The home-made SNOM used for such study was set operating in air in collection mode with a fixed oblique angle of illumination (θ=45°). Different illumination wavelengths ranging from visible to near infrared were used. Home-made procedure for tip manufacturing was based on chemical etching process producing tips with an aperture diameter of nearly 50nm. After the etching process, the tip are coated by a tiny metallic (evaporated aluminum) layer so as to prevent light from coupling into the fiber from anywhere other than at the aperture of the probe. In figure 1, we summarize the results experimentally obtained for the identification of gold nanoshells inside mouse cells making use of an aperture SNOM [10]. In the central image of figure 1, the overlapping of the topography of the mouse cell and the optical map collected by the SNOM shows two dark points evidenced by the arrows. Such dark points correspond to a strong reduction of the collected signal by the SNOM. This is due to the high external light absorption of the NSs plasmons interacting with the external e.m. field.

Fig. 1. (Left), 20μm×20μm topography of h9c2 mouse cell recorded with a home-made aperture SNOM; (middle) an overlapping of the topography image with the correspondent optical map, the arrows denote the NS identified within the cell; (right), strong-absorption points marked by arrows in the overlapping image and denoting the dimensions of the NSs. (Adapted with permission from [10]).

The penetration depth of NIR light in animal cells is very high. To have an idea of how thick the cell layer must be in order to absorb the light the extinction coefficient of the animal cell (h9c2 mouse cell in our case) is a key parameter. The penetration depth, h, as a function of wavelength can be estimated by the relation $h \approx 1/\text{Im}\left\lfloor\sqrt{\varepsilon_{cell}(\omega)}\right\rfloor$. Being the imaginary component of the cell dielectric function negligible, the penetration depth can reach to centimeters for a wavelength falling in the NIR range. Our single cell measurements as represented in figure 1, showed a topography with a height of nearly 3μm so that all the cell is practically transparent to external NIR source light.

The measurements whose results are reported in figure 1, lead to a fundamental question: which is the height of the NS inside the cell, we will define this problem as the *z-location* question. Before to detail on the analytical and numerical approach, essentially based on the dyadic Green function method to solve such problem, we must clarify some aspects connected to the numerical strategy.

A Finite Domain Time Difference (FDTD) simulation model was applied to analyze the near-field properties around the irradiated nanoparticles [18]. This computational technique is commonly recognized to give an adequate picture of the electromagnetic field distribution in the near and far-fields around structures with arbitrary shapes. The main signal observed in the FDTD simulation is the Poynting vector of the evanescent wave. Since the *z* component of the Poynting vector is also the collected signal by the SNOM, the FDTD simulation gives a results that can be immediately compared with the experimental results. However, the observed intensity collected by the SNOM aperture tip needs a comment. As I_{inc} we choose the incident intensity, averaged over the cross-sectional area of the SNOM aperture tip perpendicular to the Poynting vector (**S**=**E**×**H**) of the evanescent wave, that is spatially characterized by a penetration depth d_p corresponding to the *z*-height of collecting volume available to the SNOM aperture. Therefore due to rapid decay of electric fields in *z*-direction, one additional useful parameter to describe the optical profiles as measured by the SNOM could be the *z* dependence of the near field intensity dI/dz. In our FDTD results we will calculate this quantity.

In turn, the near-field approximation needs an additional consideration. In far-field approximation, to exhibit the relative absorption and scattering ability of the NSs, the cross sections for absorption and scattering can be defined as $\sigma_{abs}=W_{abs}/I_{inc}$ and $\sigma_{scat}=W_{scat}/I_{inc}$ respectively, while the efficiencies are defined as $Q_{abs}=\sigma_{abs}/A$ and $Q_{scat}=\sigma_{scat}/A$, for the absorption and the scattering processes, respectively. Here, if the I_{inc} represents the intensity of the incident wave, $A=\pi r^2$ is the particle cross-section projected onto a plane perpendicular to the incident wave, and *r* is the total radius on the nanosphere.

Finally, the absorption and scattering energy $W_{abs/scat}$ can be calculated using the Poynting vector integrating on all a solid angle [19]; on the contrary, in near-field, if we consider a finite dimension of tip aperture, we have that the scattered and absorbed intensity are proportional to the solid angle [20-23].

Therefore, the near-field solution of electric and magnetic fields and the field enhancement in *z*-direction in proximity of the SNOM probe tip, under some specific conditions, can provide intense locally enhanced absorption. Since the E_z components under the SNOM tip is about 10 times larger compared to the in-plane components [24-26], it is reasonable to suppose that when the probe signal displays a point-like absorption peaks, this can be identified with a nanoshell [10]. This is because the field enhancement caused by the local surface plasmon resonance mainly focuses on the metal-dielectric interface (and decays exponentially) is not absorbed by the biological tissue due to the NIR transparency window.

3. THE *z*-LOCATION PROBLEM OF NPs INSIDE A CELL: THE NEAR-FIELD APPROACH.

The *z*-localization of a NS inside the cell requires near-field approach to calculate the scattering cross-section. In particular, we have to consider that the *observer* is the SNOM aperture that we consider as

circular ring located few nanometers over the cells being scanned. We refer to this question as the *z-location problem*. In the scattering analysis we have to assume that the NS embedded within the film is small compared to the wavelength. This condition is satisfied because our NSs fall in 100-150nm diameter range, while the wavelength used is 780nm. Under this condition it is widely known that the NS scatters light like an electric point dipole radiates. It is well known that the scattered electric field from the particle can be calculated using the Green's dyadic function as

$$E_s(r) = \frac{k_0^2}{\varepsilon_0} G(r, r_0) \cdot p_0 \qquad (1)$$

where E_s is the electric field scattered at the position r in presence of a point-like dipolar source p_0 located at r_0, ε_0 is the free-space permittivity, k_0 the free wavenumber and $G(r, r_0)$ is the Green's tensor associated with the whole system. We are assuming that the nanoshell and the background are nonmagnetic ($\mu=1$), with a relative permittivity, ε and ε_B, respectively. The dyadic Green's function is defined by

$$\nabla \times \nabla \times G(r, r') - k_0^2 \varepsilon(r) G(r, r') = \delta(r - r') \qquad (2)$$

Thus, if the induced dipole moment is known the scattered electric field E_s can be easily obtained via the dyadic Green's function. The coordinate system is cylindrical and characterized by choosing the center of the scattering NS particle as $r' = r_0 = z_0 \hat{z}$.
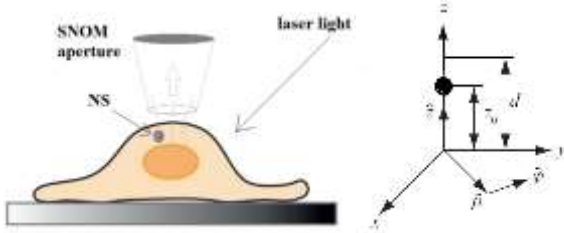

Figure 2. (Left) schematic sketch representing the cell+NS sample with the aperture SNOM and, (right) the cylindrical systems of coordinates, where d is the potential penetration depth, and z_0 is the localization of the NS with respect to the ground. $d-z_0$ is the distance between NS and SNOM probe.

The local density of plasmonic modes generated by the nanoparticles can be quantified by

$$\rho(r, \omega) = \frac{1}{\pi \omega^2 k_0^2 \varepsilon_0} \mathrm{Im}[G(r, r')] \qquad (3)$$

In terms of Green's dyadic function, the scattered field E can be obtained by the incident field E_0 via the 3D expression

$$E(r) = E_0(r) + k_0^2 \iiint G(r, r') \cdot \Delta \varepsilon E_0(r') dr' \qquad (4)$$

where $\Delta \varepsilon = \varepsilon(r) - \varepsilon_B$, and ε_B is the dielectric constant of the substrate. The Eq. (4), can be used to compute the Green's function by solving the self-consistent Dyson's equation [27]

$$G(r, r') = G_0(r, r') + k_0^2 \iiint G_0(r, r'') \cdot \Delta \varepsilon \cdot G_0(r'', r') dr'' \qquad (5)$$

To calculate the scattered part of the electric field in the upper- or substrate we used the dyadic Green's functions $G^>(r, r')$ and $G^<(r, r')$ for $r > z_0$ and $r < z_0$, respectively. In the next sections, we present the near-field dyadic Green's functions following the calculations derived by Jung et al. [28]. Following Jung et al. [28], the dyadic Green's function $G^>(r, r')$ and $G^<(r, r')$ may be expressed in cylindrical coordinate (ρ, φ, z) as

$$G_i^{(s)}(r, r_0) = \frac{-i}{4\pi} \int_0^\infty d\kappa_\rho \frac{e^{\pm i\kappa_{z_i} z}}{\kappa_{z_i}} \xi_{+,i}^{(s)}(\kappa_\rho, z_0, d) \left[\frac{J_0'(\kappa_\rho \rho)}{\rho} \hat{\rho}\hat{\rho} + \kappa_\rho J_0''(\kappa_\rho \rho) \hat{\varphi}\hat{\varphi} \right] \qquad (6.a)$$

$$G_i^{(p)}(r, r_0) = \frac{i}{4\pi k_i^2} \int_0^\infty d\kappa_\rho \frac{e^{\pm i\kappa_{z_i} z}}{\kappa_{z_i}} \left\{ \xi_{+,i}^{(p)}(\kappa_\rho, z_0, d) \left[\frac{\kappa_\rho^3 J_0'(\kappa_\rho \rho)}{\kappa_{z_i}} \hat{z}\hat{z} \pm i \frac{\kappa_\rho^2 \kappa_{z_i} J_0''(\kappa_\rho \rho)}{\kappa_{z_1}} \hat{\rho}\hat{z} \right] \right.$$
$$\left. + \xi_{-,i}^{(p)}(\kappa_\rho, z_0, d) \left[-\kappa_{z_i} \kappa_\rho J_0''(\kappa_\rho \rho) \hat{\rho}\hat{\rho} - \kappa_{z_i} \frac{J_0'(\kappa_\rho \rho)}{\rho} \hat{\varphi}\hat{\varphi} \pm i\kappa_\rho^2 J_0'(\kappa_\rho \rho) \hat{\rho}\hat{z} \right] \right\} \qquad (6.b)$$

where J_n is the nth–order Bessel function of the first kind, and the primes on the Bessel functions imply derivative with respect to the argument. d is the distance between the NS and SNOM probe aperture, $\kappa_{z_1} = \sqrt{k_i^2 - \kappa_\rho^2}$. The factors $\xi_{\pm,i}^{(x)}(\kappa_\rho, z_0, d)$ are expressed as

$$\xi_{\pm,>}^{(x)}(\kappa_\rho, z_0, d) = \frac{t_>^{(x)}\left[e^{i\kappa_z(d-z_0)} \pm r_<^{(x)} e^{i\kappa_z(d+z_0)} \right]}{1 - r_>^{(x)} r_<^{(x)} e^{2i\kappa_z d}} e^{-i\kappa_z d} \qquad (7.a)$$

$$\xi_{\pm,<}^{(x)}(\kappa_\rho, z_0, d) = \frac{t_<^{(x)}\left[e^{i\kappa_z z_0} \pm r_>^{(x)} e^{i\kappa_z(2d-z_0)} \right]}{1 - r_>^{(x)} r_<^{(x)} e^{2i\kappa_z d}} \qquad (7.b)$$

where $r^{(x)}$ denotes the Fresnel reflection coefficients for s and p polarization given by, respectively,

$$r_>^{(s)} = \frac{\kappa_z - \kappa_{z_{><}}}{\kappa_z + \kappa_{z_{><}}} \qquad r_>^{(p)} = \frac{\varepsilon_{><} \kappa_z - \varepsilon_g \kappa_{z_{><}}}{\varepsilon_{><} \kappa_z + \varepsilon_g \kappa_{z_{><}}}$$

so that the transmission coefficients become $t_>^{(x)} = 1 + r_>^{(x)}$. Near-field absorption properties of a gold NP require some assumptions as already mentioned, in particular, the speed of light approaching to infinity. Thus $\kappa_{z_1} = \sqrt{k_i^2 - \kappa_\rho^2} \to i\kappa_\rho$ and $r_>^{(s)} \to 0$ $r_>^{(p)} \to \alpha_{><}$, where α is a factor connected to the plasmon resonance [29]. Using these approximations, the near- field dyadic Green's function [28]

$$G_>^{(p)}(r, r_0) = \frac{i}{4\pi k_>^2} \int_0^\infty d\kappa_\rho \kappa_\rho^2 e^{\kappa_\rho z} \left\{ \xi_{+,>}^{(p)}(\kappa_\rho, z_0, d) \left[J_0(\kappa_\rho \rho) \hat{z}\hat{z} + J_0'(\kappa_\rho \rho) \hat{\rho}\hat{z} \right] \right.$$
$$\left. + \xi_{-,>}^{(p)}(\kappa_\rho, z_0, d) \left[J_0''(\kappa_\rho \rho) \hat{\rho}\hat{\rho} + \frac{J_0'(\kappa_\rho \rho)}{\kappa_\rho \rho} \hat{\varphi}\hat{\varphi} + J_0'(\kappa_\rho \rho) \hat{\rho}\hat{z} \right] \right\} \qquad (9)$$

with

$$\xi_{\pm,>}^{(p)}(\kappa_\rho, z_0, d) = (1-\alpha_>) \cdot \left(e^{-\kappa_\rho z_0} \mp \alpha_< e^{-\kappa_\rho(2d-z_0)} \right) \sum_{n=0}^{\infty} (\alpha_> \alpha_<)^n e^{-2\kappa_\rho nd}$$

(10)

The z dependence of the near-field intensity in the substrate can be investigated as [27]

$$I_{z>} = \int_{-\infty}^{d} dz \int_0^{2\pi} \int_0^{\infty} \rho d\rho d\varphi |\boldsymbol{E}_{z>}(\boldsymbol{r})|^2$$

(11)

where $\boldsymbol{E}_{z>}$ is calculated from Eq. (1) using the near-filed approximation of the dyadic Green's function. Since the imaginary component of the dielectric function of the cell is negligible, we assume the dipole emitter condition and the total near-field power absorbed in z direction at the edge of the SNOM probe tip as for an illuminating light of $\lambda=780$nm [28]

$$I_{abs} = \frac{\omega I_0 d^4 \operatorname{Im} \varepsilon_{cell} \varepsilon_0}{96} \sum_{l,k}^{\infty} (\alpha_> \alpha_<)^{l+k} \left\{ \frac{1}{[d(l+k)+z_0]^3} \right.$$
$$\left. + \frac{\alpha_<^2}{[d(l+k+2)-z_0]^3} - \frac{2\alpha_>}{[d(l+k+1)]^3} \right\}$$

12

The numerical results on the NS z-location question implied in Eq. (11-12) will be presented and discussed in the next section. It must be evidenced that Eq. (12) takes in account only the contribution of the evanescent wave in z-direction because the Poynting vector, and hence energy flow, is along an orthogonal direction with respect to z.

4. NUMERICAL RESULTS AND DISCUSSION

Here, we provide a numerical demonstration of how the near-field approximations of the dyadic Green's function can be used to quantify the electric field at the edge of the SNOM probe tip when the optical response of a NS particle is dominated by near-field absorption. The absorption characteristic of gold nanoshell has been shown in [10]. The NS is considered as a vertical dipole located at z=0, and d is the distance between the NS and the SNOM aperture. The distance d is composed by d_1 that is the thickness layer of the cell and d_2 that is the distance between the SNOM probe and the cell. We assume that the distance d_2 is known and equal to 10nm, commonly considered as a reasonable value of the probe-sample distance in our SNOM. The SNOM aperture cannot be considered a point, being its diameter approximately 50nm in respect with the dimension of the NS that is around 120nm. Such dimensions imply that we have to consider lateral fields in the total sum of the absorbed fields in z direction. Now, we apply the formalism of Green's method presented in the previous section to obtain the numerical results. The method used is equivalent to the Discrete Dipole Approximation DDA method [17]. All the system composed by the NS, the cell substrate and the aperture SNOM, as reported in figure 2, is discretized with rectangular parallelepipeds of dimensions $a \times b \times c$. We set the a, b, c parameters as $a=b=c=$1nm. Using Eq. (12), we calculate the electric field intensity in z direction for the basin NIR wavelength, relevant for our previous experimental results, i.e. $\lambda=$780nm. The distance between SNOM aperture and the cell upper edge is set to 10nm, for sake of simplicity we consider air ($\varepsilon=1$) between the SNOM aperture and the cell. The position of the NS inside the cell is a variable that can change continuously in the range 10-400nm and the position of the NS is taken on its upper edge.

One basic contribution of this paper is the accurate determination of the z location of the NS inside the cell. This can be made gaining a deep knowledge on the penetration depth d_p of the collected light from the aperture SNOM. The z decay of a s- or p-polarized electric field is $\sim\exp(-z/d_p)$. The penetration depth expresses the value of z where the amplitude of the electric filed is reduced by a factor $1/e$. The value of d_p is independent of the polarization of the incident light and decrease with the angle of incident light. In our experiment, a fixed angle of incidence of $\theta=45°$ was used for all the measurements. The z component of the electric field is calculated from Eq. (11) and shown in figure 3. The resulting penetration depth d_p is $\sim$100nm. The dipole approximation is considered adequate because, following the DDA approach, only the upper part of the NS is divided into many pieces with similar distance to the SNOM aperture and then make a summation. For a small spherical particle this should correspond to a dipole emitter at a distance of $z_0 \sim r$, where r is the NS radius.
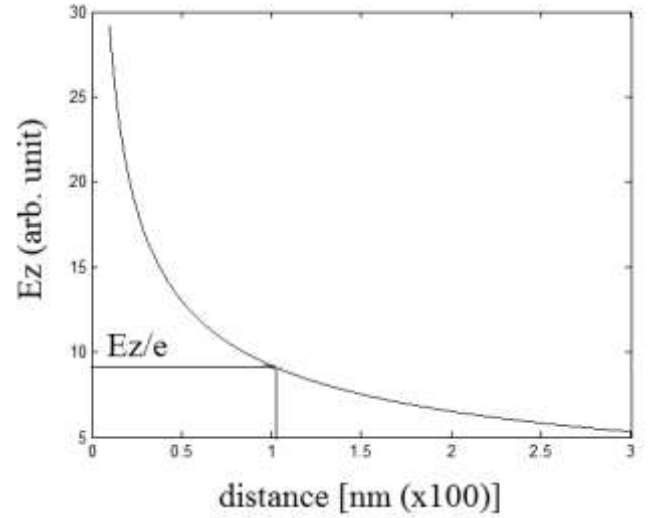

Figure 3. Calculation of SNOM penetration depth d_p as a function of the SNOM aperture-NS upper part. The SNOM aperture is 50nm diameter, the wavelength $\lambda=$780nm, the incidence angle is $\theta=45°$.

Figure 3 shows that the penetration depth available to the aperture SNOM is $\sim$100nm. To have an immediate representation of this result and its implications for investigations in biology in the NIR transparency windows, we could image that the volume inside the cell from which the SNOM probe collected the optical signal is a cylinder-like with the base coincident to the SNOM aperture and an height correspondent to the penetration depth d_p. The map of dI/dz, that is the z- derivative of Eq.(12) is shown in figure 4 using a FDTD method based on a Matlab code written ad hoc [18].
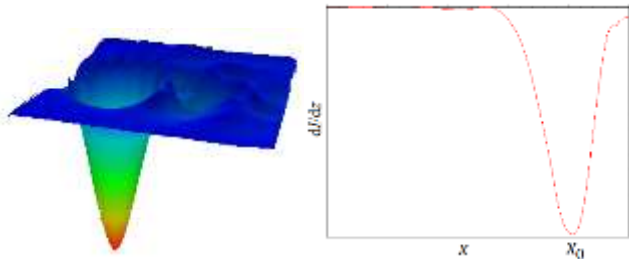
Figure 4. Left, map of signal dI/dz as collected by the aperture SNOM as a function of spatial coordinate xy for a barium titanate-gold NS of 120nm (80nm+40nm) diameter. The map is made considering the NS located z=100nm far from the SNOM probe. Right, profile of dI/dz as a function of the scanning line x, x_0 denotes the spatial position of the NS. The minimum of dI/dz is reached in correspondence of the NS particle position. All the units are arbitrary.

The intense variation of dI/dz in correspondence of the NS position is in excellent agreement with experimental results displayed in figure 1. This results is particularly meaningful. It demonstrated that inside the penetration depth, the optical signal that corresponds to the total quantity of photons collected by the aperture probe reaches a drastic reduction when the probe is positioned just above the NS.

Figures 3 and 4 represent the original contribution of the present paper. We have demonstrated that when an animal cell is illuminated by NIR light, the transparency window gives the possibility to identify metal nanoparticles when their absorption is particularly intense in the NIR region inside a penetration depth of the cell of approximately 100nm. Indeed, the cellular membrane which delimits the boundaries of the cell's body, has a thickness of about 10-15nm, so any deeper detection below the cell surface must be considered to be intracellular. Our simulation gives confirmation about the experimental results gained using an aperture SNOM. The general analytical and numerical approach used in the present paper can be employed in a wide range of SNOM applications. The extension of our analysis to scattering SNOM is immediate. This result is particularly important for the design of NSs to be applied in hyperthermia cancer treatments [30]. However, other investigations involving near-field plasmonics, biological systems and scanning optical microscopy can take advantage by our results. In particular, new methods of detection and precise localization of smart nanoparticles, such as these NSs, could disclose promote remarkable spill-overs in the emerging field of nanobiomedicine.

5. CONCLUSIONS

Most biological soft tissues have a relatively low light absorption coefficient in the NIR regions, characteristic known as the tissue optical window. Over such window, near infrared light transmits through the tissues with the scattering-limited attenuation and minimal heating preventing the healthy tissues to be damaged. In this paper, starting from some experimental results previously obtained by our group on the identification of gold NSs inside mouse cells, we numerically demonstrate that an aperture SNOM is able to locate such nanoparticles inside cells with a depth of about 100nm. This result has been obtained developing a numerical task based on the calculation of the dyadic Green function in near-field approximation. This result is particularly significant because it gives an accurate knowledge of the depth distance for the analysis of the optical properties inside cells under the near infrared transparency window. This feature is due to a combination of two properties: the NIR transparency of biological systems and the strong absorption capability of appropriate size gold nanoshells in the near-infrared range. Our results can stimulate further developments in the field of thermal treatments of cancers or near-field plasmonics investigation of biological systems.

References

1. S. A. Maier, Plasmonics: Fundamentals and Applications, Springer, 2007.
2. K. L. Kelly, E. Coronado, L.L. Zhao, G.C. Schatz, "The Optical Properties of Metl Nanoparticles: The Influence of Size, Shape and Dielectric Environment", J. Phys. Chem. B, **107**, 668 (2003).
3. V. Myroshnychenko, J. Rodríguez-Fernández, I. Pastoriza-Santos, A. M. Funston, C. Novo, P. Mulvaney, L. M. Liz-Marzan, and F. J. García de Abajo, "Modelling the optical response of gold nanoparticles", Chem. Soc. Rev., **37**, 1792 (2008).
4. J. B. Jackson, S.L. Westcott, L.R. Hirsch, J.L. West, N.J. Halas, "Controlling the surface enhanced Raman effect via the nanoshell geometry", Appl. Phys. Lett., **82**, 257 (2003).
5. W.E. Doering, M.E. Piotti, M.J. Natan, R.G. Freeman, "SERS as a Foundation for Nanoscale, Optically Detected Biological Labels", Advanced Materials, **19**, 3100, (2007).
6. A. Cricenti, "Scanning Near-Field Optical Microscopy (SNOM)", Physica Status Solidi C, **5**, 2615 (2008).
7. L.R. Hirsch, A.M. Gobin, A. R. Lowery, F. Tam, R.A. Drezek, N.J. Halas, J.L. West, "Metal nanoshells", Ann. Biomed. Eng., **34**, 15 (2006).
8. W. Chen, C. Ayala-Orozco, N.C. Biswal, C. Perez-Torres, M. Bartels, R. Bardhan, G. Stinnet, X-D. Liu, B. Ji, A. Deorukhkar, L.V. Brown, S. Guha, R. G. Pautler, S. Krishnan, N.J. Halas, A. Joshi, "Targeting of Pancreatic Cancer with Magneto-Fluorescent Theranostic Gold Nanoshells", Nanomedicine. **9**, 1209 (2016)
9. C, Liu, C.C. Mi, B.Q. Li, "Energy absorption of gold nanoshells in Hyperthermia therapy", IEEE Transactions of Nanobioscience, **7**, 206 (2008).
10. M. D'Acunto, A. Cricenti, S. Dinarelli, M. Luce, "Optical detection of core-gold nanoshells inside Biosystems", NanoSpectroscopy, **1**(1), 97 (2015).
11. D. Sarkar, N.J. Halas, "General vector basis function solution of Maxwell's equations", Physical Review E, **56**, 1102 (1997).
12. D. Le, "SURE Project, Spectroscopic Characterization of Silica-Gold Nanoshells", available at http://www.cmmp.ucl.ac.uk/~mdl/cam/Mie/nanoshells.pdf
13. J. Feng, V. C. Siu, A. Roelke, V. Metha, S. Y. Rhieu, G. T. R. Palmore, D. Pacifici, "Nanoscale Plasmonic Interferometers for Multispectral, High-throughput Biochemical Sensing", Nano Letters, **12**, 602 (2012).
14. P. Fan, U. K. Chettiar, L. Cao, F. Afshinmanesh, N. Engheta, M. L. Brongersma, "An invisible metal-semiconductor photodetector", Nature Photonics, **6**, 380 (2012).
15. C. Wu, X. Liang, H. Jiang, "Metal nanoshells as a contrast agent in near-infrared diffuse optical tomography", Optics Communications , **253** , 214 (2005).
16. G. Mie, "Beiträge zur Optik trüber Medien, speziell kolloidaler Metallösungen", Ann. Phys. (Leipzig), **25**, 377 (1908).
17. M. D'Acunto, D. Moroni, O. Salvetti, "Nanoscale Biomolecular Detection Limit for Gold Nanoparticles Based on Near-Infrared Response", Advances in Optical Technologies, (2012)

18. A. Cricenti, M. Luce, D. Moroni, O. Salvetti, M. D'Acunto, "Ultrasmall clusters of gold nanoshells detected by SNOM"; Optoelectronics Review **23**, 39 (2015)

19. M. D'Acunto, A. Cricenti, M. Luce, S. Dinarelli, "Theory of near-field detection of core-gold nanoshells inside biosystems", Computer Modelling & New Technologies, **19,** 29 (2015).

20. R. Wannemacher, M. Quinten, A. Pack, "Evanescent-wave scattering in near-field optical microscopy", Journal of Microscopy, **194**, 260 (1999).

21. M. Quinten, A. Pack, R. Wannemacher, "Scattering and extinction of evanescent waves by small particles", Appl. Physics B **68**, 87 (1999).

22. M. Quinten, "Evanescent wave scattering by aggregates of clusters- application to optical near-field microscopy", Appl. Physics B, **70**, 579 (2000).

23. A.Y. Bekshaev, K.Y. Bliokh, F. Nori, "Mie scattering and optical forces from evanescent fields: A complex-angle approach", Optics Express, **21**, 7982 (2013).

24. A. Cricenti, V. Marocchi, R. Generosi, M. Luce, P. Perfetti, D. Vobornik, G. Margaritondo, D. Talley, P. Thielen, J. S. Sanghera, I.D. Aggarwal, J.K. Miller, N.H. Tolk, D. W Piston, "Optical nanospectroscopy study of ion-implanted silicon and biological growth medium", Journal of Alloys and Compounds, **362**, 21 (2004).

25. F. Keilmann, R. Hilenbrand, "Near-filed microscopy by elastic light scattering from a tip", Philosophical Transactions, Series A, Mathematical, physical and engineering sciences, **362**, 787 (2004)

26. P. Dvořák, T. Neuman, L. Břínek, T. Šamoril, R. Kalousek, P. Dub, P. Varga, T. Šikola, NanoLetters, Control and Near-Field Detection of Surface Plasmons Interference Patterns, **13**, 2558, (2013).

27. Y. Ould Agha, O. Demichel, C. Girard, A Bouelier, G. Colas des Francs, "Near-field properties of plasmonics nanostructures with high aspect ratio", arXiv: 1509.07103v1, 2015

28. J. Jung, T. Søndergaard, T. G. Pedersen, K. Pedersen, A. Nylandsted Larsen, B. B. Nielsen, Phys. Rev. B., "Dyadic Green's functions of thin films: Applications within plasmonics solar cells", **83**, 085419 (2011).

29. J. Jung, T. G. Pedersen, T. Søndergaard, K. Pedersen, A. N. Larsen, B. B. Nielsen, Phys. Rev. B., " Electrostatic plasmon resonances of metal nanospheres in layered geometries", **81**, 125413 (2010).

30. D. Sikdar, I. D. Rukhlenko, W. Cheng, M. Premaratne, "Effect of number density on optimal design of gold nanoshells for plasmonic photothermal therapy", Biomedical Optics Express, **4**, 15 (2013)